Reports

Hydrothermal Plume Measurements: A Regional Perspective

EDWARD T. BAKER AND GARY J. MASSOTH

An extensive deep-tow survey around an active submarine vent field was conducted to map the three-dimensional distribution of hydrothermal emissions and calculate the hydrothermal discharge of heat and manganese. Emissions from the 10-kilometer-long vent field formed a nearly isopycnal plume about 250 meters thick and elongated in the direction of the local net current. Net export of hydrothermal discharge from both point and diffuse sources was estimated from the advective transport of the plume; the heat flux was 5.8 ± 2.9 × 10^8 watts and the dissolved manganese flux was 0.2 ± 0.1 moles per second. Flux measurements of this type could be expanded to encompass entire ridge segments, allowing comparison with theoretical thermal and chemical process models on a common spatial scale.

SEAWATER CIRCULATING THROUGH hot and newly formed ocean crust at mid-ocean spreading centers exits the ocean floor in buoyant plumes carrying heat and chemicals from the underlying basalt (*1*). The most visible results of this transfer process are vent chimneys and clusters created in the axial valleys of spreading centers when dissolved constituents in the ascending fluids rapidly precipitate as they are mixed with and cooled by the ambient seawater. Submersible-based observations and sampling at specific vent orifices provide indispensable information on the chemical (*2, 3*) and heat (*4, 5*) content of vent fluids. Because of the scarcity of available measurements and the diversity of emission types on the seafloor, however, such point sampling may adequately describe neither the distribution nor flux of hydrothermal emissions on a vent-field scale. The inherent limitations of individual vent measurements prompted us to begin a complementary regional approach, first mapping the three-dimensional distribution of an integrated plume from an entire vent field and then calculating the total point and diffuse flux of certain hydrothermal constituents by measuring the advective transport of the plume itself.

We here apply this approach to a well-developed plume emanating from a 10-km section of ridge along the top of a 70-km morphological dome centered at 44°44′N, 130°20′W on the southern Juan de Fuca Ridge in the northeast Pacific Ocean. Six active vent sites have been identified on the floor of the axial valley in this area (*6*), and three high-temperature sites have been sampled (*3*). Each sampled site discharged fluid through multiple point sources (chimneys) and extensive diffuse leakage. The structure of the resulting hydrothermal plume was mapped by an acoustically navigated instrument package (*7*) regularly cycled through the bottom 200 to 400 m while towed from a surface ship (*8*). Real-time measurements of temperature and particle-concentration anomalies determined the location and intensity of the plume in the water column. The temperature anomaly, ΔT, is the temperature in excess of that predicted for a given potential density (σ_θ) surface by a plot of σ_θ against potential temperature (Θ). This relation is linear at ridge-crest depths except where influenced by nonmixing processes such as hydrothermal or conductive heating. Light attenuation values in excess of the regional midwater minimum identified particle concentration anomalies.

A series of six tows conducted during 14 days in June 1985 defined the three-dimensional distribution of hydrothermal emissions around the vent sites. Emerging vent fluids mix with ambient seawater in the axial valley to form a plume 100 to 200 m thick that is vertically rather uniform except within about 1 km of a vent. This layer, the diluted hydrothermal plume, has a σ_θ range

National Oceanic and Atmospheric Administration, Pacific Marine Environmental Laboratory, Seattle, WA 98115-0070.

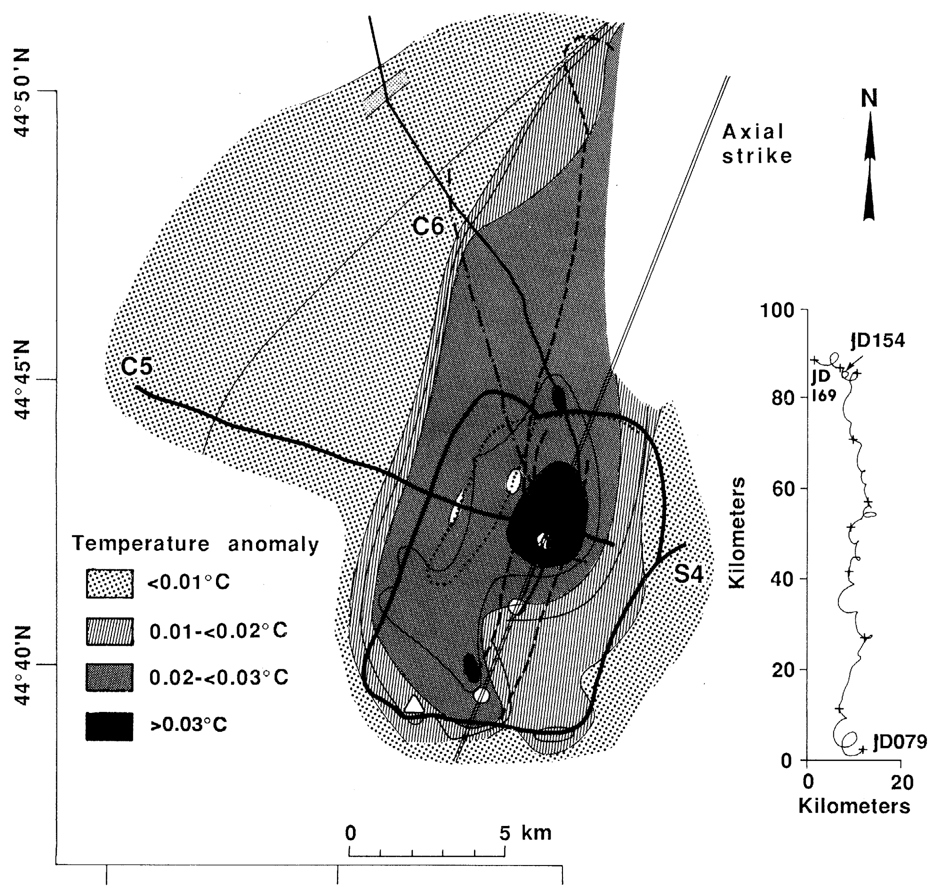

Fig. 1. Areal map of the hydrothermal plume on the 27.70 σ_θ (~2050 m) surface. Tow paths are shown by dashed, dotted, or heavy solid lines. The axial valley is a flat-floored depression 2 to 3 km wide and 80 to 100 m deep centered on the "axial strike" line. The temperature anomaly is contoured at 0.005°C intervals and shaded at 0.01°C intervals. Locations of the current meter (△) and the sampled vent sites (○) are shown. A progressive vector diagram describes the regional current flow before (JD079-JD154) and during (JD154-JD169) the survey period. All known active vent sites within this map area lie within tow S4.

of 27.698 to 27.702 kg/m^3, so that its distribution can be mapped by an areal plot of ΔT on the 27.70 σ_θ surface (Fig. 1). The resulting map reveals considerable temperature variability on the isopycnal surface: ΔT maximums and steep gradients above the known vent locations, a broad, horizontally asymmetric zone with low or almost nonexistent ΔT gradients, and sharp lateral boundaries with ΔT gradients as steep as 0.02°C per kilometer. Cross-axis tows C5 and C6 also encountered a secondary thermal (and particle) plume centered on the 27.07 σ_θ surface. Because this density surface nowhere intersects the axial valley, the ΔT anomaly apparently represents an off-axis hydrothermal vent located at a depth of at least 2300 m on the ridge flank. We conclude from Fig. 1 that the high-temperature vent fluids are diluted by a factor of about 8500 (340°C/0.040°C) within tens of meters of their source and that the resultant plume undergoes much slower dilution as it is advected by the regional flow. The direction of net flow for 3 months before the end of the survey, as measured by a current meter moored 100 m above the west axial wall on the 27.70 σ_θ (2030 m) surface was 353°, virtually coincident with the apparent axis of the plume (Fig. 1).

The vertical distribution of the temperature anomaly is shown by a three-dimensional view constructed from tow S4 that encircled the known vent locations (Fig. 2). The core of the primary plume, identified by $\Delta T > 0.02$°C and centered on the 27.70 σ_θ surface, is uniformly about 100 m thick between the axial valley and the sharp lateral boundary to the west. Vertical temperature (and particle) gradients characteristically are much steeper above the plume than below.

The flux of a conservative hydrothermal constituent from the vent field equals the net advective transport of that constituent within the plume, assuming that the plume is a steady-state feature and that diffusive transport is negligible. Several observations support these assumptions. The uniform plume distribution during the 2-week survey period, coupled with the long-term consistency of the current flow (Fig. 1), implies that the plume distribution had been stationary for at least 3 months. This interval is much longer than the 10-day residence time of a water parcel in the vent field, calculated as the quotient of the length of the vent field and the mean current velocity along the plume axis [0.0105 ± 0.0053 m/sec (*9*)]. Mean velocity normal to the plume axis was not statistically significant, so we neglect flux in that direction. The existence of sharp temperature gradients along the lateral boundaries of the plume indicates that diffusive transport also is low normal to the axis.

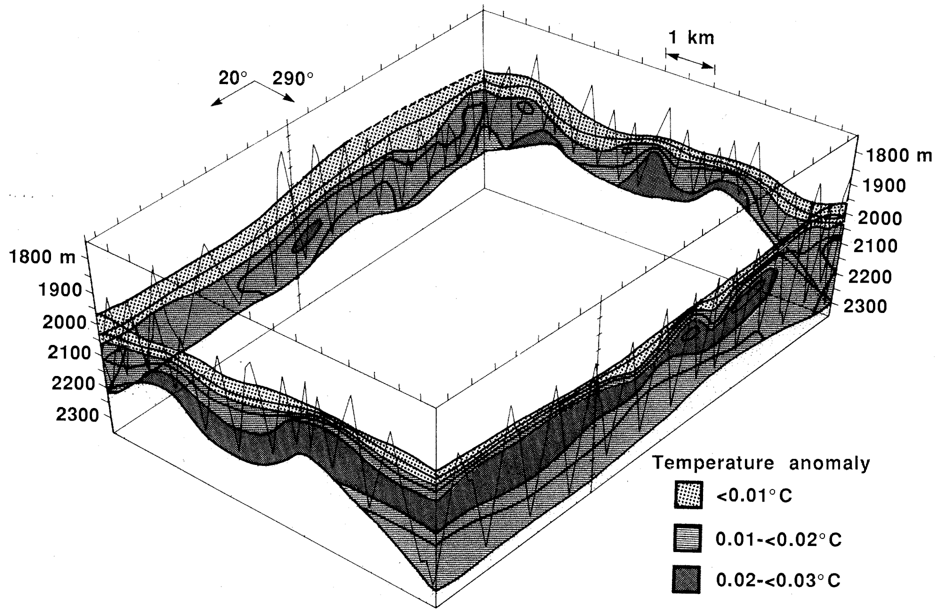

Fig. 2. Three-dimensional representation of the hydrothermal plume based on tow S4. The view is roughly looking upcurrent. The tow path is shown by the saw-tooth curve along each panel. Note the well-mixed nature of the plume water in the bottom 100 to 150 m of the axial valley and the very weak horizontal temperature gradients in the core of the plume.

The flux of hydrothermal heat (Q) is the product of the net heat anomaly within a vertical cross section normal to the plume axis and the along-axis plume velocity. The heat anomaly

$$H = \rho C_p[\Sigma A_i(\Delta T_i - \Delta T_b)]$$

where ΔT_i is the temperature anomaly and A_i is the area between isotherms on a 10-km cross section constructed from tows S4 and C5; ΔT_b is 0.01°C, the background ΔT advected into the vent field area from the south; and specific heat $\rho C_p = 4.2 \times 10^6$ J/m^3°C. The hydrothermal heat source is then

$$Q = (0.0105 \pm 0.0053 \text{ m/sec}) \, (5.7 \times 10^{10} \text{ J/m})$$

Total heat loss from the 10-km-long vent field (approximately circumscribed by tow S4) is thus $5.8 \pm 2.9 \times 10^8$ W. Previous estimates of hydrothermal heat generated at this site range from 5×10^7 to more than 40×10^7 W/km of ridge axis (*10*), but these were based only on temperature anomalies from a single along-axis deep tow and simplistic plume models.

Our measured heat loss per kilometer of ridge axis is about a factor of 7 higher than the theoretical heat loss by hydrothermal circulation within 3 km of the axis on the southern Juan de Fuca Ridge (*11*). This inequality is appropriate if vent fields concentrate along the shallowest section of ridge segments (*12*), which is where our survey was located, or if hydrothermal circulation is episodic (*13*). A typical high-temperature chimney in the 21°N vent field has a heat flux of about 10^6 to 10^7 W (*5*); the 10-km section of ridge measured here might thus support about 10 to 100 such chimneys, or many fewer if substantial heat

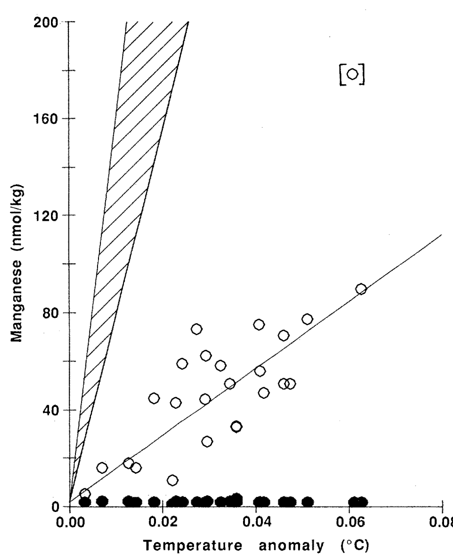

Fig. 3. Temperature anomaly as a function of dissolved (○) and particulate (●) Mn in the plume. Least-squares regression of DMn has a slope of 1.4 ± 0.1 nmol/cal, excluding the anomalous bracketed point. The range of DMn/heat ratios for vent water (*14*), here back-extrapolated by a factor of about 10^{-4}, is given by the shaded area. Particulate Mn was a minor component of the total Mn everywhere in the plume regions discussed here. Particulate Mn was determined by thin-film x-ray fluorescence spectrometry of samples filtered onto 0.4-μm pore size filters. Dissolved Mn was determined by atomic absorption spectrophotometry following concentration with 8-hydroxyquinoline (*16*). All analytical errors are less than 15% of the determined value.

loss occurs through diffuse fluid leakage. An accurate accounting of point-source heat losses could be used to gauge the scale of diffuse heat leakage where the total heat flux of a vent field was known.

For a nonconservative constituent, the advective transport in the plume equals that fraction of the original hydrothermal discharge which escapes the vent field (this fraction may be greater than 1 and may change with distance from the vent field, as for the particulate phase of a continually precipitating chemical species). The flux of total suspended particles through the northern boundary of the vent field, for example, was 94 ± 48 g/sec.

The flux of constituents that can be sampled only discretely may be estimated from their correlation with the continuously measured temperature or particle concentration. Samples of dissolved manganese (DMn) from throughout the plume, for example, exhibit a linear relation with ΔT (Fig. 3), giving a slope of 1.4 ± 0.1 nmol/cal and implying a total vent field flux of DMn of 0.2 ± 0.1 mol/sec. The DMn to heat ratios of high-temperature fluids at this site apparently range from 7.6 to 15.7 nmol/cal, however, because of extremely high concentrations of DMn [up to 4.5 mmol/kg (*14*)]. The approximate order of magnitude difference between DMn to heat ratios in the vent fluids and the diluted plume implies either that the reported high-temperature samples (*14*) are not representative of the integrated emissions of the entire vent field, or that 80 to 90% of the DMn is scavenged from the vent emissions during formation of the plume. Furthermore, the low and uniform particulate Mn in the plume (Fig. 3) requires that any scavenged Mn be deposited before the scavenging particles become entrained in the plume. Analogous inconsistencies have been observed near the 21°N vent fields, where the total dissolvable $Mn/^3He$ ratio in vent waters is about twice that in the plume waters (*15*).

Even though the origin of such inconsistencies is presently obscure, their existence indicates that a limited set of individual vent samples may not adequately represent the regional composition and flux of hydrothermal emissions. A regional view also clarifies the interpretation of time-dependent processes such as precipitation and scavenging in the plume, since samples collected along the advective path will appear to "age" much more slowly than samples collected across the plume boundaries. Finally, this approach can be readily expanded from vent-field to ridge-segment size, thereby enabling the measurement of hydrothermal flux on a spatial scale that will more appropriately reflect the scale of current geophysical models.

REFERENCES AND NOTES

1. R. F. Weiss, P. Lonsdale, J. E. Lupton, A. E. Bainbridge, H. Craig, *Nature (London)* **267**, 600 (1977); J. B. Corliss *et al.*, *Science* **203**, 1073 (1979); RISE Project Group, *ibid.* **207**, 1421 (1980); J. M. Edmond, K. L. Von Damm, R. E. McDuff, C. I. Measures, *Nature (London)* **297**, 187 (1982).
2. J. M. Edmond *et al.*, *Earth Planet. Sci. Lett.* **46**, 1 (1979); Canadian American Seamount Expedition, *Nature (London)* **313**, 212 (1985); K. L. Von Damm *et al.*, *Geochim. Cosmochim. Acta* **49**, 2197 (1985).
3. U.S.G.S. Juan de Fuca Study Group, *Geology*, in press.
4. K. C. Macdonald, K. Becker, F. N. Spiess, R. D. Ballard, *Earth Planet. Sci. Lett.* **48**, 1 (1980).
5. D. R. Converse, H. D. Holland, J. M. Edmond, *ibid.* **69**, 159 (1984).
6. J. R. Delaney, H. P. Johnson, J. L. Karsten, *J. Geophys. Res.* **86**, 11747 (1981); W. R. Normark, J. L. Morton, R. A. Koski, D. A. Clague, J. R. Delaney, *Geology* **11**, 158 (1985).
7. The instrument package consisted of a hydrodynamically faired Sea Bird CTD (conductivity-temperature-depth) coupled to a Sea Tech transmissometer with a 0.25-m path length. CTD resolution was ±0.00004 S/m and ±0.0003°C.
8. E. T. Baker, J. W. Lavelle, G. J. Massoth, *Nature (London)* **316**, 342 (1985).
9. Mean velocity along the plume axis is the component along 20° of the 2.86-hour-filtered 90-day current meter record. The standard error estimate is $\pm\sigma/(T/\tau)^{0.5}$, where σ = standard deviation of the current meter record, T = record length, and τ = an independent time scale [J. S. Allen and P. K. Kundu, *J. Phys. Oceanogr.* **8**, 13 (1978)] estimated as the area under the autocorrelation function for a particular record.
10. K. Crane *et al.*, *J. Geophys. Res.* **90**, 727 (1985).
11. J. L. Morton and N. H. Sleep, *ibid.*, p. 11345.
12. R. D. Ballard and J. Francheteau, *Mar. Tech. Soc. J.* **16**, 8 (1982).
13. K. C. Macdonald, *Annu. Rev. Earth Planet. Sci.* **10**, 155 (1982); N. H. Sleep, J. L. Morton, L. E. Burns, T. J. Wolery, in *Hydrothermal Processes at Seafloor Spreading Centers*, P. A. Rona, K. Bostrom, L. Laubier, K. L. Smith, Eds. (Plenum, New York, 1983), pp. 53–82.
14. K. Von Damm and J. L. Bischoff, *Eos* **66**, 926 (1985). The high end ratio was computed from the maximum DMn concentration and the single reported temperature of 284°C; the low end ratio from the minimum DMn concentration and the maximum expected temperature of 340°C.
15. J. E. Lupton *et al.*, *Earth Planet. Sci. Lett.* **50**, 115 (1980).
16. G. P. Klinkhammer, *Anal. Chem.* **52**, 117 (1980).

17. Supported by the NOAA VENTS program. We thank J. R. Delaney, S. Hammond, J. W. Lavelle, and H. Curl, Jr., for thoughtful reviews, and G. Lebon, K. Roe, and D. Tennant for technical assistance.

9 June 1986; accepted 6 October 1986

A Common Mechanism of Chromosomal Translocation in T- and B-Cell Neoplasia

LAWRENCE R. FINGER, RICHARD C. HARVEY, ROBERT C. A. MOORE, LOUISE C. SHOWE, CARLO M. CROCE

The chromosomal breakpoint involved in the t(8;14)(q24;q11) chromosome translocation in the SKW-3 cell line, which directly involves the 3′ flanking region of the c-*myc* gene, was cloned and sequenced. The breakpoint on chromosome 8 mapped to a position 3 kb 3′ of c-*myc* while the chromosome 14 breakpoint occurred 36 kb 5′ of the gene for the constant region of the α chain of the T-cell receptor (TCR). The translocation resulted in a precise rearrangement of sequences on chromosome 8 and what appears to be a functional J_α segment on chromosome 14. Signal sequences for V-J joining occurred at the breakpoint positions on both chromosomes 14 and 8, suggesting that the translocation occurs during TCR gene rearrangement and that it is catalyzed by the enzymatic systems involved in V-J joining reactions. The involvement of c-*myc* in the translocation and the association of joining signals at the breakpoints provides a parallel to the situation observed in the translocations involving c-*myc* and the immunoglobulin loci in B-cell neoplasms and suggests that common mechanisms of translocation and oncogene deregulation are involved in B- and T-cell malignancies.

MOST HUMAN T-CELL NEOPLASMS carry specific chromosomal rearrangements, predominantly chromosomal translocations and inversions. These rearrangements frequently involve chromosome 14 at band q11 (*1–4*) where the locus for the α chain of the T-cell receptor (TCR) resides. The α locus of the TCR (TCR-α) is split in T-cell leukemias carrying the t(11;14) chromosome translocation (*5*). The genes for the variable (V_α) regions are proximal to the breakpoints and remain on chromosome 14 while the gene for the constant region (C_α) translocates to chromosome 11 (*5*). In T-cell leukemias carrying a t(8;14)(q24;q11) chromosome translocation, the C_α locus translocates to a region 3′ to the c-*myc* oncogene (*6*). The translocation-associated c-*myc* gene is deregulated in Burkitt lymphomas (*7*) and a c-*myc* involved in a translocation with the TCR-α locus is similarly deregulated (*6*).

Both the t(11;14)(q13;q32) and the t(14;18)(q32;q21) chromosome translocations associated with specific B-cell neoplasms predominantly involve immunoglobulin heavy-chain J regions (*8*). In addition,

The Wistar Institute, Philadelphia, PA 19104.